Biol Trace Elem Res (2014) 157:84–93
DOI 10.1007/s12011-013-9871-9

Reactive Oxygen Species-Mediated DNA Damage and Apoptosis in Human Skin Epidermal Cells After Exposure to Nickel Nanoparticles

Saud Alarifi · Daoud Ali · Saad Alakhtani · Entissar S. Al Suhaibani · Ahmed A. Al-Qahtani

Received: 21 October 2013 / Accepted: 27 November 2013 / Published online: 6 December 2013

Abstract Nickel nanoparticles (NiNPs) are increasingly used in various applications due to their unique properties. However, there is little information concerning the toxicity of NiNPs in the human skin cell (A431). The present study was designed to investigate the cytotoxicity, apoptosis, and DNA damage due to NiNPs in A431 cells. A cellular proliferative capacity test showed that NiNPs induce significant cytotoxicity in a dose- and time-dependent manner. NiNPs were also found to induce oxidative stress evidenced by the generation of reactive oxygen species (ROS) and depletion of glutathione (GSH). Further, co-treatment with the antioxidant *N*-acetylcysteine (NAC) mitigated the ROS generation due to NiNPs, suggesting the potential mechanism of oxidative stress. NiNPs also induced significant elevation of lipid peroxidation, catalase, and superoxide dismutase and caspase-3 activity in A431 cells. In addition, NAC suppressed NiNP-induced caspase-3 activity. DNA fragmentation analysis using the comet assay showed that the NiNPs cause genotoxicity in a dose- and time-dependent manner. Therefore, the study points out the capability of the NiNPs to induce oxidative stress resulting in apoptosis and genotoxicity. This study warrants more careful assessment of NiNPs before their industrial applications.

Keywords Nickel nanoparticles · Human skin epithelial cells · Oxidative stress · Apoptosis · DNA damage

Daoud Ali and Saud Alarifi contributed equally to this work.

S. Alarifi · D. Ali (✉) · S. Alakhtani · E. S. Al Suhaibani
Department of Zoology, College of Science, King Saud University, Box 2455, Riyadh 11451, Saudi Arabia
e-mail: daudali.ksu12@yahoo.com

D. Ali
e-mail: aalidaoud@ksu.edu.sa

A. A. Al-Qahtani
Department of Infection and Immunity, Research Center, King Faisal Specialist Hospital & Research Center, Riyadh, Saudi Arabia

Introduction

Nickel is a widely distributed metal which is applied in many forms. These broad applications, however, increase human and environmental exposure and thus the potential risk related to their toxicity. Approximately 10 % of the population in the USA suffers from nickel allergy, and many others are unable to wear jewelry or handle coins and other objects that contain nickel [1, 2]. Some researches have been developed to reduce the penetration of nickel through the skin, but few formulations are safe and effective [2]. There are some significant studies evaluating the toxic potential of nickel nanoparticles (NiNPs). NiNPs caused cytotoxicity and apoptosis in mouse epidermal JB6 cells. [3]. Guo et al. [4] reported the cytotoxic effects of NiNPs in leukemia cancer cells. Due to the growing number of applications, there is an increasing risk of environmental exposure to nanomaterials. Their potential toxicological impacts are still a matter of investigation, and our actual knowledge on the effects of engineered nanosized contaminants on biological systems remains incomplete [5, 6]. These effects need to be assessed in order to provide a scientific basis for safe development of nanotechnologies. Due to their small size, as nanoparticles (NPs) may cross biological barriers to reach different tissues according to their surface and size properties, accumulation of metal NPs was previously observed in many different organs [7].

Free oxygen radical generation and oxidative stress elicit a wide variety of cellular events including DNA damage and apoptosis [8]. The genotoxic potential of nanomaterials is of particular concern since the changes of the genetic material

have potential for cell death, tissue malfunction, cancer development, and adverse reproductive effects. The skin is the largest organ of the body and could serve as an important portal route for entry of NPs in the human body. Oxidative stress has been implicated as an explanation behind nanoparticle toxicity [9]. Recent studies reported nanoparticle-induced oxidative stress as determined by increasing membrane lipid peroxidation (LPO), reactive oxygen species (ROS), and decreasing intracellular glutathione [10]. We evaluated the oxidative stress biomarkers including reduced glutathione (GSH) as an antioxidant; ROS generation as a collective marker of superoxide anion (O_2^-), hydroxyl radical (HO·), and hydrogen peroxide (H_2O_2); and malondialdehyde (MDA) as an end product of membrane LPO in response to NiNP exposure.

Therefore, the present study was done to assess the cellular toxicity and genotoxic potential of NiNPs in human skin epidermal cells as well as to understand its possible mechanism.

Materials and Methods

Chemicals and Reagents

Nickel nanopowder (NiNPs) (CAS number 7440-02-0, product no. 577995, and APS <100 nm), GSH, 5,5-dithio-bis-(2-nitrobenzoic acid) (DTNB), MTT [3-(4,5-dimethylthiazol-2-yl)-2,5-diphenyltetrazolium bromide], *N*-acetylcysteine (NAC), 2,7-dichlorofluorescin diacetate (DCFH-DA), and propidium iodide were obtained from Sigma-Aldrich. Fetal bovine serums, penicillin–streptomycin, and DMEM/F-12 medium were purchased from Invitrogen Co. (Carlsbad, CA, USA). All other chemicals used were of the highest purity and available from commercial sources.

Nickel Nanoparticle Preparation and Characterization

NiNPs were suspended in Milli-Q water at a concentration of 1 mg/ml. Stock suspension was probe-sonicated at 40 W for 15 min. The average hydrodynamic size of NiNPs was measured by dynamic light scattering (DLS) (Nano-Zeta Sizer-HT, Malvern Instrument, UK), and DLS experiments were performed as described by Murdock et al. [11].

Samples for transmission electron microscopy (TEM) analysis were prepared by drop-coating the NiNP solution on carbon-coated copper TEM grids. The films on the TEM grids were allowed to dry prior to measurement. Field emission transmission electron microscopy (FETEM, JEM-2100 F, JEOL Inc.) was used to characterize the size and shape of NiNPs at an accelerating voltage of 200 kV.

Cell Culture and Exposure to NiNPs

The human skin epithelial cell line (A431) was procured from American Type Culture Collection Rockville, MD, USA, and it was preserved and subcultured in the laboratory and was used to determine the cytotoxicity of NiNPs. Cells were cultured in DMEM/F-12 medium supplemented with 10 % FBS and 100 U/ml penicillin–streptomycin at 5 % CO_2 and 37 °C. At 85 % confluence, cells were harvested by using 0.25 % trypsin and were subcultured into 75-cm^2 flasks, 6-well plates, and 96-well plates according to experiments. Cells were allowed to attach to the surface for 24 h prior to treatment. NiNPs were suspended in the cell culture medium and diluted to appropriate concentrations (2, 4, 8, and 20 μg/ml). The appropriate dilutions of NiNPs were then sonicated using a sonicator bath at room temperature for 10 min at 40 W to avoid particle agglomeration before exposure to the cells. Cells not exposed to NiNPs served as control in each experiment.

To investigate the role of ROS and caspase-3 activity, the cells were exposed to NiNPs with and without 5 mM *N*-acetylcysteine for 24 h.

Cell Morphology

The morphology of A431 cells was observed after exposure to different concentrations of NiNPs for 24 and 48 h by using a phase-contrast microscope (Leica DMIL).

MTT Assay

MTT assay was used to investigate mitochondrial function as described by Mossman [12]. Briefly, 1×10^4 cells/well were seeded in 96-well plates and exposed to different concentrations (2, 4, 8, and 20 μg/ml) of NiNPs for 24 and 48 h. At the end of the exposure, culture media were replaced with new media containing the MTT solution (0.5 mg/ml) and incubated for 4 h at 37 °C. As a result, formazan crystal was formed and it was dissolved in dimethyl sulfoxide (DMSO). The plates were kept on a shaker for 10 min at room temperature and then analyzed at 530 nm using a multiwell microplate reader (Omega Fluostar). Untreated sets were also run under identical conditions and served as controls.

Lactate Dehydrogenase Leakage Assay

The release of cytoplasmic lactate dehydrogenase (LDH) enzyme into the culture medium was determined by Wroblewski and LaDue [13]. A431cells were treated with different concentrations (2, 4, 8, and 20 μg/ml) of NiNPs for 24 and 48 h. After exposure, 100-μl samples from the centrifuged culture media were collected. The LDH activity was assayed in 3.0 ml of reaction mixture with 100 μl of pyruvic acid (2.5 mg/ml phosphate buffer) and 100 μl of nicotinamide adenine

dinucleotide (NADH; 2.5 mg/ml phosphate buffer), and the rest of the volume was adjusted with phosphate buffer (0.1 M, pH 7.4). The rate of NADH oxidation was determined by following the decrease in absorbance at 340 nm for 3 min at 1-min intervals at 25 °C using a spectrophotometer (Varian-Cary 300 Bio). The amount of LDH released is expressed as LDH activity (IU/l) in culture media.

Measurement of Intracellular Reactive Oxygen Species

ROS generation was assessed in A431 cells after exposure to different concentrations (2, 4, 8, and 20 μg/ml) of NiNPs by using 2,7-dichlorofluorescin diacetate (DCFH-DA) dye as fluorescence agent [14]. ROS generation was studied by two methods: fluorometric analysis and microscopic fluorescence imaging. For fluorometric analysis, cells (1×10^4 per well) were seeded in 96-well black bottom culture plates and allowed to adhere for 24 h in a CO_2 incubator at 37 °C. Then, A431 cells were exposed to the above concentrations of NiNPs for 24 and 48 h. On the completion of respective exposure periods, cells were incubated with DCFH-DA (10 mM) for 30 min at 37 °C. The reaction mixture was aspirated and replaced by 200 μl of PBS in each well. The plates were kept on a shaker for 10 min at room temperature in the dark. Fluorescence intensity was measured using a multiwell microplate reader (Omega Fluostar) at an excitation wavelength of 485 nm and emission wavelength of 528 nm, and values were expressed as percentage of fluorescence intensity relative to control wells.

A parallel set of cells (5×10^4 per well) was analyzed for intracellular fluorescence using an upright fluorescence microscope equipped with a CCD cool camera (Nikon Eclipse 80i equipped with Nikon DS-Ri1 12.7 megapixel camera).

Oxidative Stress Biomarkers

Cells with a final density of ~6×10^6 in a 75-cm^2 culture flask were exposed to different concentrations (0, 2, 4, 8, and 20 μg/ml) of NiNPs for 24 and 48 h. After exposure, the cells were scraped and washed twice with chilled 1× PBS. The harvested cell pellets were lysed in cell lysis buffer [20 mM Tris–HCl (pH 7.5), 150 mM NaCl, 1 mM Na_2EDTA, 1 % Triton, and 2.5 mM sodium pyrophosphate]. The cells were centrifuged at 15,000×*g* for 10 min at 4 °C, and the supernatant (cell extract) was maintained on ice until it was assayed for oxidative stress biomarkers. Protein content was measured using the method of Bradford [15], using bovine serum albumin as the standard.

Lipid Peroxidation Assay

The extent of membrane LPO was estimated by measuring the formation of MDA using the method of Ohkawa et al. [16]. MDA is one of the products of membrane LPO. A mixture of 0.1 ml of cell extract and 1.9 ml of 0.1 M sodium phosphate buffer (pH 7.4) was incubated at 37 °C for 1 h. The incubation mixture, after precipitation with 5 % TCA, was centrifuged (2,300×*g* for 15 min at room temperature), and the supernatant was collected. Then, 1.0 ml of 1 % TBA was added to the supernatant and placed in boiling water for 15 min. After cooling to room temperature, the mixture was observed at 532 nm and expressed in nanomoles of MDA per hour per milligram of protein using a molar extinction coefficient of 1.56×10^5 M/cm.

Glutathione Estimation

GSH level was quantified using Ellman's reagent [17]. The assay mixture contained phosphate buffer, DTNB, and cell extract. The reaction was monitored at 412 nm, and the amount of GSH was expressed in terms of nanomoles of GSH per milligram of protein.

Measurement of Superoxide Dismutase

Superoxide dismutase (SOD) activity was estimated by employing a method described by Kakkar et al. [18]. The assay mixture contained sodium pyrophosphate buffer, nitroblue tetrazolium (NBT), phenazine methosulphate (PMS), reduced NADH, and the required volume of the cell extract. One unit of SOD enzyme activity is defined as the amount of enzyme required for inhibiting chromogen production (560 nm) by 50 % in 1 min under assay conditions and expressed as specific activity in units per minute per milligram of protein.

Measurement of Catalase Activity

Catalase (CAT) activity was measured by following its ability to split hydrogen peroxide (H_2O_2) within 1 min of incubation time. The reaction was then stopped by adding dichromate/acetic acid reagent, and the remaining H_2O_2 was determined by measuring chromic acetate at 570 nm which is formed by reduction of dichromate/acetic acid in the presence of H_2O_2 as described earlier by Sinha [19]. CAT activity was expressed as micromoles of H_2O_2 decomposed per minute per milligram of protein.

Quantification of Apoptosis Using Ethidium Bromide and Acridine Orange

NiNPs induced cell death in A431 cells, and it was quantified by using ethidium bromide (EtBr) and acridine orange (AO) double staining according to standard procedures and was examined under a fluorescence microscope (Leica attached with Q-Fluor software) [20]. Briefly, cells were seeded at a

concentration of 1×10^4 cells/ml in a 30-mm cell culture plate and after 24 h treated with NiNPs (8.0 μg/ml). Then, cell culture plates were incubated in an atmosphere of 5 % CO_2 at 37 °C for 48 h. At the end of exposure, the cells were spun down at 1,000 rpm for 10 min. The supernatant was discarded, and the cells were washed twice with phosphate buffer saline after centrifuging at 1,000 rpm for 10 min to remove the medium. Fluorescent dyes containing AO (10 μg/ml) and EtBr (10 μg/ml) were added into the cell culture plate. A freshly stained cell suspension was dropped on a glass slide and covered with a cover slip. Slides were observed under a fluorescence microscope within 30 min before the fluorescence color starts to fade. The percentage of viable and apoptotic cells was determined in 200 cells. AO and EtBr are intercalating nucleic acid-specific fluorochromes which emit green and orange fluorescence, respectively, when they are bound to DNA. Viewed by fluorescence microscopy, viable cells appear to have a green nucleus with intact structure, while apoptotic cells exhibit a bright green nucleus showing condensation of chromatin as dense green areas. Late apoptotic cells and necrotic cells will stain with both AO and EtBr. Hence, late apoptotic cells exhibited an orange nucleus showing condensation of chromatin, while necrotic cells display an orange nucleus with intact structure.

Caspase-3 Assay

The activity of caspase-3 was determined from the cleavage of the caspase-3 substrate I (*N*-acetyl-DEVD-*p*-nitroaniline). *p*-Nitroaniline was used as the standard. Cleavage of the substrate was monitored at 405 nm, and the specific activity was expressed in picomoles of the product (nitroaniline) per minute per milligram of protein.

Determination of DNA Strand Breakage

The alkaline single cell gel electrophoresis (SCGE) was performed as a three-layer procedure with slight modification [21, 22]. In brief, 70,000 cells/well were seeded in a six-well plate. After 24 h of seeding, cells were treated with different concentrations of NiNPs for 24 and 48 h. After treatment, the A431 cells were trypsinized and resuspended in DMEM, and the cell suspension was centrifuged at 1,200 rpm at 4 °C for 5 min. The cell pellet was finally suspended in chilled phosphate buffer saline for the comet assay. Viability of cells was evaluated using the trypan blue exclusion method [23]. The samples showing cell viability higher than 84 % were further processed for the comet assay. In brief, about 15 μl of cell suspension (approximately 20,000 cells) was mixed with 85 μl of 0.5 % low melting point agarose and layered on one end of a frosted plain glass slide, pre-coated with a layer of 200 μl of normal agarose (1 %). Thereafter, it was covered with a third layer of 100 μl of low melting point agarose. After solidification of the gel, the slides were immersed in lysing solution (2.5 M NaCl, 100 mM Na_2EDTA, 10 mM Tris pH 10 with 10 % DMSO and 1 % Triton X-100 added fresh) overnight at 4 °C. The slides were then placed in a horizontal gel electrophoresis unit. Fresh cold alkaline electrophoresis buffer (300 mM NaOH, 1 mM Na_2EDTA, and 0.2 % DMSO, pH 13.5) was poured into the chamber and left for 20 min at 4 °C for DNA unwinding and conversion of alkali-labile sites to single-strand breaks. Electrophoresis was carried out using the same solution at 4 °C for 20 min, at 15 V (0.8 V/cm) and 300 mA. The slides were neutralized gently with 0.4 M Tris buffer at pH 7.5 and stained with 75 μl of ethidium bromide (20 μg/ml). For positive control, the A431cells were treated with 100 μM H_2O_2 for 10 min at 4 °C. Two slides were prepared from each well (per concentration), and 50 cells per slide (100 cells per concentration) were scored randomly and analyzed using an image analysis system (Komet-5.0, Kinetic Imaging, Liverpool UK) attached to a fluorescence microscope (DMLB, Leica, Germany) equipped with appropriate filters. The parameters, e.g., percentage of DNA in the tail (i.e., percentage tail DNA=100−percentage head DNA), were selected for quantification of DNA damage in A431cells as determined by the software.

Statistical Analysis

At least three independent experiments were carried out in duplicates for each evaluation. Data were expressed as mean (±SE) and analyzed by one-way analysis of variance (ANOVA). A p value of less than 0.01 was considered statistically significant.

Results

Nickel Nanoparticles

Figure 1a showed the typical TEM images of the NiNPs. These pictures exhibit that the majority of the particles were in a spherical shape with smooth surfaces. The TEM average diameter was calculated by measuring over 100 particles in random fields of TEM view. The average TEM diameter of NiNPs was 52.10±6.40 nm. Figure 1b represents the frequency of size (in nanometers) distribution of NiNPs.

All of the data from electron microscopy and associated techniques were obtained under high vacuum and constitute the size, morphology, and composition analysis characteristics of the NiNPs. The average hydrodynamic size and zeta potential of NiNPs in the cell culture medium determined by DLS were 67.8±2 nm and −26.60 mV.

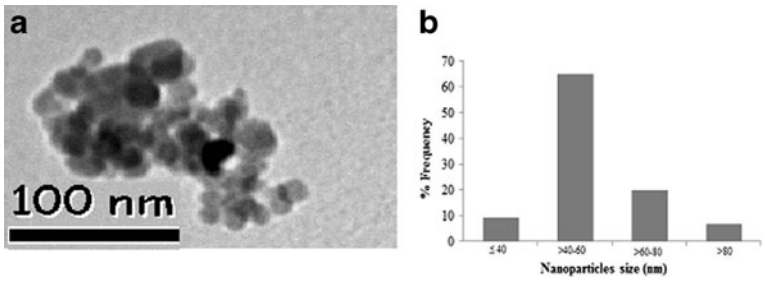

Fig. 1 Characterization of NiNPs. **a** TEM image and **b** the size distribution histogram generated by using TEM image

Morphological Changes

Figure 2 showed the comparative morphology of untreated and NiNP-treated A431 cells. Cells treated with 20 μg/ml NiNPs changed into a spherical shape and detached from the surface (Fig. 2b).

NiNPs Induced Cytotoxicity in A431 Cells

We examined the mitochondrial function (MTT reduction) and membrane damage (LDH leakage) as cytotoxicity end points. MTT results demonstrated a concentration- and time-dependent cytotoxicity after exposure to NiNPs in A431 cells (Fig. 3a). LDH release, a marker of cell membrane damage, was measured in human skin epidermal A431 cells exposed to NiNPs at concentrations of 2, 4, 8, and 20 μg/ml for 48 h. However, as the concentration of NiNPs increased, a significant LDH leakage was observed in a dose- and time-dependent manner (Fig. 3b).

Nickel Nanoparticles Induced ROS Generation and Oxidative Stress

The ability of NiNPs to induce oxidative stress was evaluated by measuring the levels of ROS, LPO, GSH, SOD, and catalase in A431 cells. Results showed that NiNPs induced intracellular ROS generation in a dose- and time-dependent

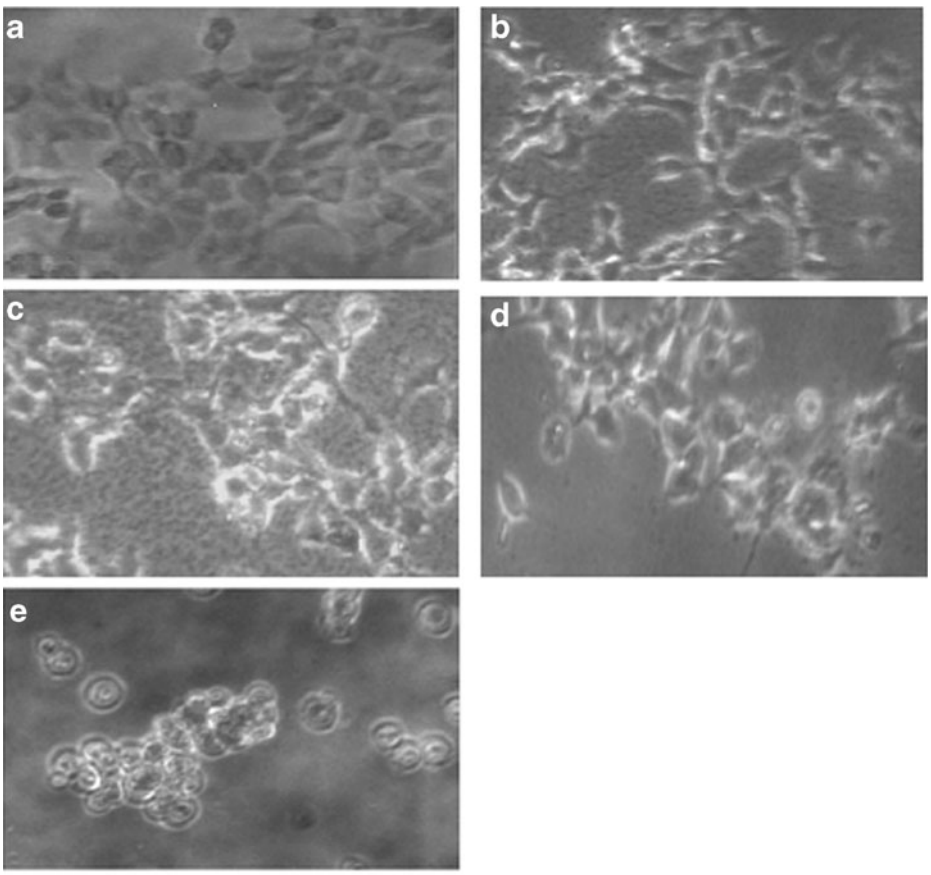

Fig. 2 Morphology of human skin epithelial cells (A431) after exposure to NiNPs for 48 h. **a** Control, **b** at 2 μg/ml, **c** at 4 μg/ml, **d** at 8 μg/ml, and **e** at 20 μg/ml

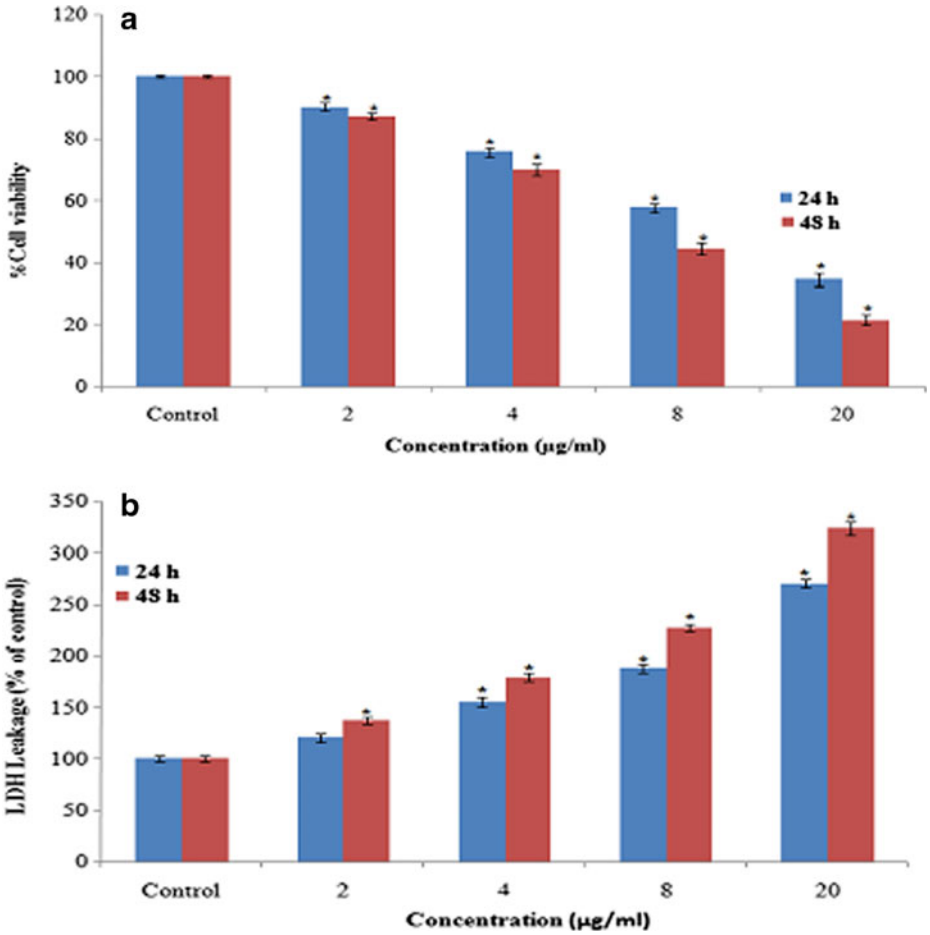

Fig. 3 Cytotoxicity of NiNPs on A431 cells for 24 and 48 h. **a** Percentage cell viability. **b** LDH leakage. Each value represents the mean±SE. of three experiments. *p <0.01 vs. control

manner (Fig. 4). We further observed that co-exposure to *N*-acetylcysteine effectively prevented the ROS generation induced by NiNPs (Fig. 4d). NiNP-induced oxidative stress was further evidenced by depletion of GSH (Fig. 5a) and elevation of LPO, SOD, and catalase with concentrations and time of NiNP exposure (Fig. 5b–d).

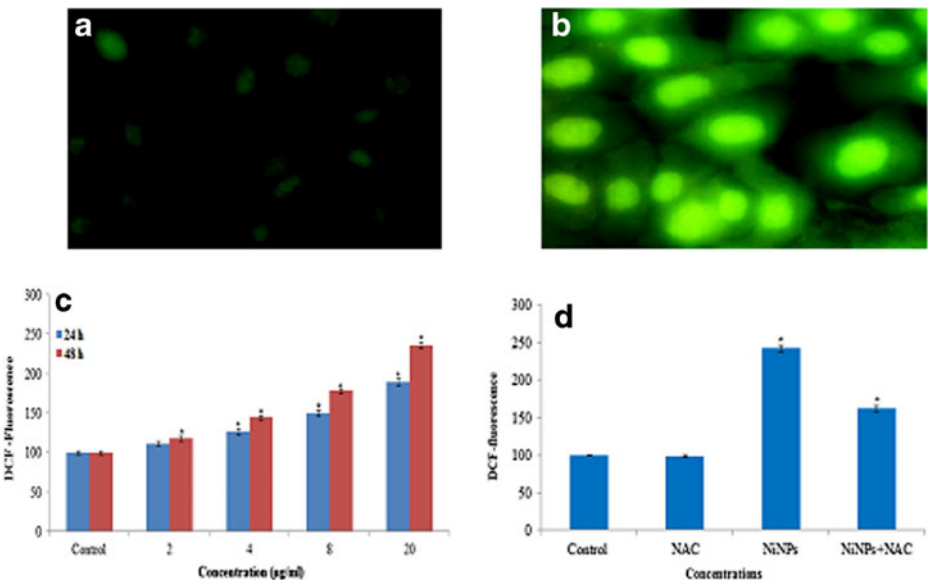

Fig. 4 NiNPs induced ROS generation in A431 cells. Images were snapped using a Nikon phase-contrast cum fluorescence microscope (model 80i). **a** Control. **b** At 8 µg/ml of NiNPs. **c** Percentage of ROS generation at different concentrations of NiNPs in A431 cells. **d** Effect of *N*-acetylcysteine on nickel nanoparticle (20 µg/ml)-induced ROS generation in A431 cells. Each value represents the mean±SE. of three experiments. *p <0.01 vs. control

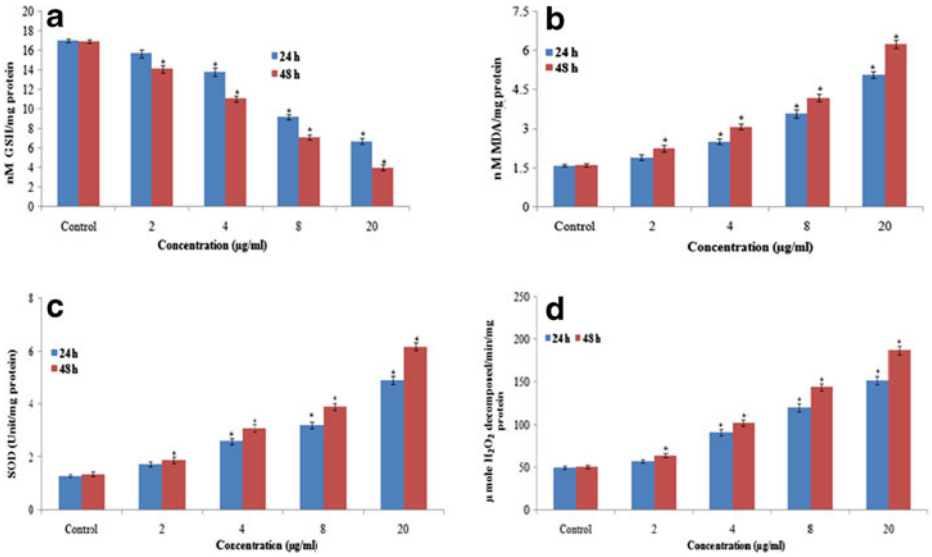

Fig. 5 **a** Levels of GSH. **b** Lipid peroxides (LPO). **c** SOD. **d** Catalase in A431 cells after exposure to NiNPs for 24 and 48 h. Each value represents the mean±SE. of three experiments.*$p<0.01$ vs. control

Apoptosis Induction by Nickel Nanoparticles

Apoptotic and viable cells were scored under a fluorescence microscope. The study revealed that NiNPs triggered morphological features relating to the occurrence of apoptosis (Fig. 6a, b). The untreated cells were observed with a green intact nuclear structure (Fig. 6a). In addition, late stages of apoptosis such as apoptotic body separation and presence of a reddish orange color due to the binding of AO to denatured DNA were observed (Fig. 6b).

Caspase-3, which plays a key role in the apoptotic pathway of cells, was induced following the treatment with NiNPs (Fig. 6c). When cells were treated with 2, 4, and 8 µg/ml concentrations of NiNPs for 24 and 48 h, the activity of caspase-3 was increased in a concentration- and time-dependent manner. On the other hand, treatment with NAC resulted in protection against NiNP-induced cell apoptosis, with the caspase3 activity decreased (Fig. 6d).

DNA Damage

DNA damage was measured as percentage tail DNA in the control as well as exposed cells. The cells exposed to different concentrations of NiNPs exhibited significantly ($p>0.01$) higher DNA damage than those of control groups. The gradual nonlinear increase in DNA damage was observed in cells as the dose and time of NiNP exposure increased. The highest DNA damage was recorded at 8 µg/ml NiNPs in A431 cells (Fig. 7).

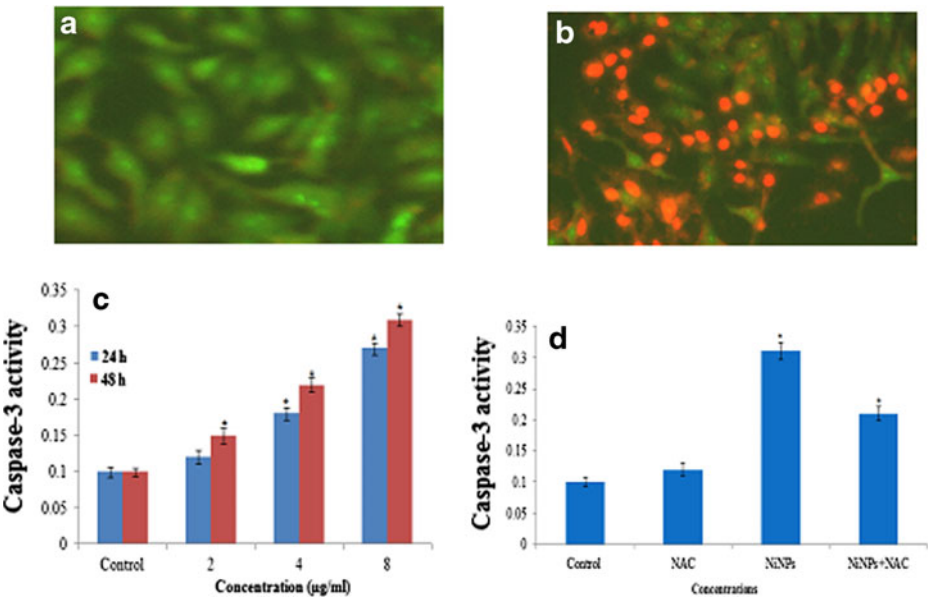

Fig. 6 Induction of apoptosis in A431 cells after NiNP exposure for 24 and 48 h. **a** Control (viable) cell. **b**. Exposed at 8 µg/ml of NiNPs. **c**. Caspase-3 activity. **d** Effect of *N*-acetylcysteine on nickel nanoparticle (8 µg/ml)-induced caspase 3 activity in A431 cells. Each value represents the mean±SE of three experiments. *$p<0.01$ vs. control

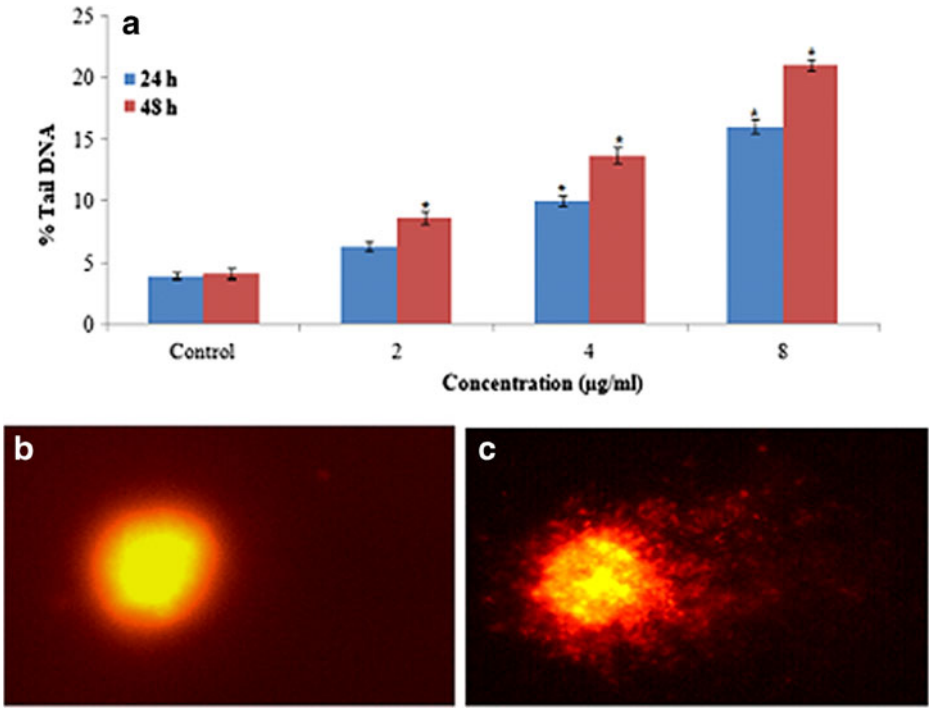

Fig. 7 DNA damage in A431 cells at different concentrations of NiNPs. **a** Percentage tail DNA. **b** Control cell. **c** Exposed cell at 8 μg/ml of NiNPs. Each value represents the mean±SE of three experiments. *$p<0.01$ vs. control

Discussion

The present study reveals the effect of NiNPs on human skin cells and provides significant insight into the possible mechanism by which NiNPs exert their toxic effect in human skin epidermal cells (A431). Our results demonstrate that NiNPs have cytotoxic and genotoxic effects on A431 cells. Our results also revealed that the mode of cell death was apoptosis which was mediated by the ROS-triggered mitochondrial pathway as evidenced by cleavage of caspase-3.

Prior to studying the genotoxic and cytotoxic potential of NiNPs, we have characterized its zeta potential and size by DLS as well as TEM. However, the size obtained from DLS was more than the size measured by TEM. The difference in size is due to the fact that different size determination methods give different results based on these principles employed: first, DLS measures Brownian motion and subsequent size distribution of an ensemble collection of particles in the solution and gives the mean hydrodynamic diameter which is usually larger than the TEM diameter as it includes a few solvent layers; second, during DLS measurement, there is a tendency of particles to agglomerate in the aqueous state, thereby giving the size of clustered particles rather than individual particles; and third, it reports an intensity-weighted average hydrodynamic diameter of a collection of particles, so any polydispersity of the sample will skew the average diameter towards larger particle sizes.

The interference of some nanoparticles with commonly used cytotoxicity test systems has been well documented in the literature. Therefore, it has been suggested that the cytotoxicity of nanoparticles should be assessed with two or more independent test systems for validating the findings [24]. We have evaluated the cytotoxicity of NiNPs by two different assays, viz. the MTT and LDH release, to increase the strength of the data. In the present study, NiNPs induced cytotoxicity in a dose- and time-dependent manner as measured by the MTT and LDH assays. In the present study, cytotoxicity results agreed with the findings of Guo et al. [4] in leukemia cancer cells exposed to nickel nanoparticles.

Lipid peroxidation and oxidative stress have been cited to be among the more important mechanisms of toxicity related to nanoparticle exposure [9]. This has been attributed to their small size and large surface area which are generally thought to produce ROS and oxidative stress [25]. The NiNPs in our study also induced intracellular ROS when examined using the cell-permeable dye DCFH-DA. ROS typically include the superoxide radical (O_2^-), hydrogen peroxide (H_2O_2), and the hydroxyl radical ($HO\cdot$) which cause damage to cellular components including DNA damage and ultimately apoptotic cell death [26, 27]. This observation is consistent with the earlier studies which have shown similar effects on human leukemia cancer K562 cells [4]. We also observed an increase in lipid peroxides, SOD, and CAT and a decrease in antioxidant GSH level in A431 cells after exposure to NiNPs, which represents a marker of oxidative stress. Lipid peroxidation can further give rise to more free radicals and damage biomolecules like DNA, proteins, and lipids in conjunction with ROS. It also causes injury to the cell membrane as indicated by an increased level of lactate dehydrogenase enzyme release. The depletion of GSH in NiNP-exposed cells combined with the increased level of lipid peroxidation, SOD, and CAT indicates

that oxidative stress may be the primary mechanism for the toxicity of NiNPs in A431 cells. The NPs can induce spontaneous ROS generation at its surface, owing to their chemical and surface characteristics. They can also lead to free radical generation after their interaction with cellular components, e.g., mitochondrial damage. Another way by which ROS are generated is through the activation of the NADPH oxidase enzyme which is responsible for O_2^- production in the membrane of phagocytic cells. When free radicals get close to cellular organelles, they may oxidize and reduce macromolecules (DNA, lipids, proteins), resulting in significant oxidative damage to the cell. Nanoparticle-induced lipid peroxidation and oxidative stress lead to DNA damage and apoptosis [28]. Our results are consistent with other investigators' findings, demonstrating that metal oxide nanoparticles have the potential to induce DNA damage [29]. We found that NiNPs significantly generated toxic effects in human skin cells. NiNPs directly applied to airway epithelial cells are highly cytotoxic, causing oxidative damage and DNA lesions [27]. Ispas et al. [30] reported that NiNPs cause mortality in zebrafish.

Apoptosis is a type of programmed cell death and involves a series of biochemical events leading to cellular morphological changes and cell death. The NiNP-induced cell death observed in this study can occur by two distinct modes—apoptosis and necrosis—which can be distinguished by morphological and biochemical features. Acridine orange/ethidium bromide staining of NiNP-treated A431 cells resulted in nuclear condensation and fragmentation which is another morphological hallmark of apoptosis. Some nanoparticles owing to their small size are capable of reaching the nucleus and interact with DNA [31]. They may also exhibit an indirect effect on DNA through their ability to generate ROS. This DNA damage may either lead to carcinogenesis or cell death, thus disrupting normal cell functions. We observed the genotoxic potential of NiNPs in A431 cells in the alkaline comet assay which is capable of detecting single as well as double DNA strand breaks and alkali-labile sites even at low levels of DNA damage [32]. Martinez et al. [33] have reported that ROS are involved in DNA damage, causing damage to both purine and pyrimidine bases as well as the DNA backbone.

In conclusion, our results indicate that NiNPs possess a DNA-damaging effect on human skin epidermal cells, which may be mediated through the reactive oxygen species and oxidative stress. Our results also indicate the potential effect of nickel nanoparticles on target human skin epidermal cells which could induce cytotoxicity to skin cancer cells and suggest the possibility for applications of the nickel nanoparticles in related biomedical sciences.

Acknowledgment The authors would like to extend their sincere appreciation to the Deanship of Scientific Research at King Saud University for its funding of this research through the research group project no. RGP-VPP-180.

Conflict of Interest The authors declare no conflicting interests.

References

1. Bataille V (2004) Genetic factors in nickel allergy. Journal of Investigative Dermatology 123, xxiv–xxv. doi:10.1111/j.0022-202X.2004.23508.x
2. Vemula PK, Anderson RR, Karp JM (2011) Nanoparticles reduce nickel allergy by capturing metal ions. Nat Nanotechnol 6:291–295
3. Zhao J, Wang ZY, Liu XY, Xie XY, Zhang K, Xing B (2011) Distribution of CuO nanoparticles in juvenile carp (Cyprinus carpio) and their potential toxicity. J Hazard Mater 197:304–310
4. Guo D, Wu C, Li X, Jiang H, Wang X, Chen B (2008) In vitro cellular uptake and cytotoxic effect of functionalized nickel nanoparticles on leukemia cancer cells. J Nanosci Nanotechnol 8:2301–2307
5. Singh N, Manshian B, Jenkins GJ, Griffiths SM, Williams PM, Maffeis TG, Wright CJ, Doak SH (2009) Nanogenotoxicology: the DNA damaging potential of engineered nanomaterials. Biomater 30: 3891–3914
6. Skocaj M, Filipic M, Petkovic J, Novak S (2011) Titanium dioxide in our everyday life; is it safe? Radiol Oncol 45:227–247
7. Li Y-F, Chen C (2011) Fate and toxicity of metallic and metal-containing nanoparticles for biomedical applications. Small 7: 2965–2980
8. Ostrovsky S, Kazimirsky G, Gedanken A, Brodie C (2009) Selective cytotoxic effect of ZnO nanoparticles on glioma cells. Nano Res 2: 882–890
9. Nel A, Xia T, Madler L, Li N (2006) Toxic potential of materials at the nano-level. Science 311:622–627
10. Wang Y, Aker WG, Hwang HM, Yedjou CG, Yu H et al (2011) A study of the mechanism of in vitro cytotoxicity of metal oxide nanoparticles using catfish primary hepatocytes and human HepG2 cells. Sci Total Environ 409:4753–4762
11. Murdock RC, Braydich-Stolle L, Schrand AM, Schlager JJ, Hussain SM (2007) Characterization of nanomaterial dispersion in solution prior to in vitro exposure using dynamic light scattering technique. Toxicol Sci 101:239–253
12. Mossman T (1983) Rapid colorimetric assay for cellular growth and survival: application to proliferation and cytotoxicity assays. J. Immunol Meth 65:55–63
13. Wroblewski F, LaDue JS (1955) Lactate dehydrogenase activity in blood. Prop Soc Exp Biol Med 90:210–213
14. Wang H, Joseph JA (1999) Quantifying cellular oxidative stress by dichlorofluorescein assay using microplate reader. Free Radic Biol Med 27:612–616
15. Bradford MM (1976) A rapid and sensitive method for the quantitation of microgram quantities of protein utilizing the principle of protein-dye binding. Anal Biochem 72:248–254
16. Ohkawa H, Ohishi N, Yagi K (1979) Assay for lipid peroxides in animal tissues by thiobarbituric acid reaction. Anal Biochem 95:351–358
17. Ellman G (1959) Tissue sulfhydryl groups. Arch. Biochem Biophys 82:70–77
18. Kakkar PS, Das B, Viswanathan PN (1984) A modified spectrophotometric assay of superoxide dismutase. Ind J Biochem Biophys 21: 130–132
19. Sinha AK (1972) Colorimetric assay of catalase. Anal Biochem 47: 389–394
20. Guan T, Qin F, Du J, Geng L, Zhang Y, Li M (2007) AICAR inhibits proliferation and induced S-phase arrest and promotes apoptosis in CaSki cells. Acta Pharm Sinica 28:1984–1990

21. Singh NP, McCoy MT, Tice RR, Schneider EL (1988) A simple technique for quantization of low levels of DNA damage in individual cells. Exp Cell Res 175:184–191
22. Ali D, Ray RS, Hans RK (2010) UVA-induced cyototoxicity and DNA damaging potential of benz (e) acephenanthrylene in human skin cell line. Toxicol Lett 199(2):193–200
23. Anderson D, Yu TW, Phillips BJ, Schmerzer P (1994) The effect of various antioxidants and other modifying agents on oxygen-radical generated DNA damage inhuman lymphocytes in the comet assay. Mutat Res 307:261–271
24. Monteiro-Riviere NA, Inman AO, Zhang LW (2009) Limitations and relative utility of screening assays to assess engineered nanoparticle toxicity in a human cell line. Toxicol Appl Pharmacol 234(2):222–235
25. Xia T, Kovochich M, Brant J, Hotze M, Sempf J, Oberley T, Sioutas C, Yeh JI, Wiesner MR, Nel AE (2006) Comparison of the abilities of ambient and manufactured nanoparticles to induce cellular toxicity according to an oxidative stress paradigm. Nano Lett 6(8):1794–1807
26. Ott M, Gogvadze V, Orrenius S, Zhivotovsky B (2007) Mitochondria, oxidative stress and cell death. Apoptosis 12:913–922
27. Rana SV (2008) Metals and apoptosis: recent developments. J Trace Elem Med Biol 22:262–284
28. Kang SJ, Kim BM, Lee YJ, Hong SH, Chung HW (2009) Titanium dioxide nanoparticles induce apoptosis through the JNK/p38-caspase-8-Bid pathway in phytohemagglutinin-stimulated human lymphocytes. Biochem Biophys Res Commun 386:682–687
29. Eom HJ, Choi J (2009) Oxidative stress of CeO_2 nanoparticles via p38-Nrf-2 signaling pathway in human bronchial epithelial cell, BEAS-2B. Toxicol Lett 187:77–83
30. Ispas C, Andreescu D, Patel A, Goia DV, Andreescu S, Wallace KN (2009) Toxicity and developmental defects of different sizes and shape nickel nanoparticles in zebrafish. Environ Sci Technol 43(16):6349–6356
31. Chen M, Mikecz A (2005) Formation of nucleoplasmic protein aggregates impairs nuclear function in response to SiO_2 nanoparticles. Exp Cell Res 305(1):51–62
32. Collins AR (2004) The comet assay for DNA damage and repair: principles, applications, and limitations. Mol Biotech 26(3):249–261
33. Martinez GR, Loureiro AP, Marques SA, Miyamoto S, Yamaguchi LF, Onuki J et al (2003) Oxidative and alkylating damage in DNA. Mutat Res 544(2–3):115–127